Available online at www.sciencedirect.com
SCIENCE DIRECT®
Nuclear Physics A 727 (2003) 41–55
NUCLEAR PHYSICS A
www.elsevier.com/locate/npe

Low-energy magnetic dipole response in ^{56}Fe from high-resolution electron scattering ☆

R.W. Fearick [a,b], G. Hartung [a], K. Langanke [c], G. Martínez-Pinedo [d,e], P. von Neumann-Cosel [a,*], A. Richter [a]

[a] *Institut für Kernphysik, Technische Universität Darmstadt, 64289 Darmstadt, Germany*
[b] *Physics Department, University of Cape Town, Rondebosch 7700, South Africa*
[c] *Institute of Physics and Astronomy, University of Aarhus, DK-8000 Aarhus C, Denmark*
[d] *Institut d'Estudis Espacials de Catalunya, Edifici Nexus 201, Gran Capità 2, E-08034 Barcelona, Spain*
[e] *Institució Catalana de Recerca i Estudis Avanqts, Passeig Lluis Companys 23, E-08031 Barcelona, Spain*

Received 26 May 2003; accepted 23 July 2003

Abstract

The ^{56}Fe(e, e′) reaction has been studied for excitation energies up to about 8 MeV and momentum transfers $q \simeq 0.4$–0.55 fm^{-1} at the Darmstadt electron linear accelerator (DALINAC) with kinematics emphasizing $M1$ transitions. Additional data have been taken for $q \simeq 0.8$–1.7 fm^{-1} at the electron accelerator NIKHEF, Amsterdam. A PWBA analysis allows spin and parity determination of the excited states. For $M1$ excitations, transition strengths are derived with a DWBA analysis using shell-model form factors. The resulting $B(M1)$ strength distribution is compared to shell-model calculations employing different effective interactions. The form factor of the prominent low-lying $M1$ transition at 3.449 MeV demonstrates its dominant orbital nature. It represents a major part of the scissors mode in ^{56}Fe.

PACS: 25.30.Dh; 21.60.Cs; 27.40.+z

Keywords: ^{56}Fe(e, e′); $M1$ form factors; Shell model; Scissors mode

☆ Work supported by the DFG under contract numbers FOR 272/2-2 and 445 SUA-113/6/0-1 and by the NRF, South Africa.
* Corresponding author.
E-mail address: vnc@ikp.tu-darmstadt.de (P. von Neumann-Cosel).

0375-9474/$ – see front matter
doi:10.1016/j.nuclphysa.2003.07.016

1. Introduction

Magnetic dipole ($M1$) excitations are a subject of long-standing interest in nuclear structure. The spin and orbital currents—and their interference invoked by $M1$ transitions provide insight into a number of important problems. The spin part is closely linked to the Gamow–Teller (GT) strength from β decay or charge exchange processes because it is mediated by the same one-body operator [1]. A quenching of the spin g-factor is observed in analogy to the renormalization of the axial-vector coupling constant (see, e.g., [2,3] and references therein). $M1$ transitions are also sensitive to non-nucleonic degrees of freedom in elementary nuclear excitations [4–6]. Furthermore, a collective orbital magnetic dipole mode—the scissors mode—has been identified [7] at low excitation energies whose strength and location are intimately related to rotational properties of the nucleus (see, e.g., [8–11] and references therein).

Recently, there has been great interest into the study of GT spin–flip transitions in fp-shell nuclei, and in particular in the mass region around ^{56}Fe, because they govern the dynamics of supernova type II explosions [12]. Efforts have been made to describe the corresponding strengths and their energy distributions in state-of-the-art shell-model calculations [13–16]. One finds that the stellar interaction rates must be considerably modified with respect to simplifying assumptions used so far in supernova models of massive stars [17].

The GT_+ and GT_- strengths in ^{56}Fe have been studied with the (p, n) [18] and (n, p) [19] charge-exchange reactions, respectively. A study of the $M1$ response in ^{56}Fe serves as an interesting test of the theoretical approaches. The spin–flip part is a measure of the GT_0 component (where the subscript denotes the $T = T_0$ isospin component with T_0 being the isospin of the ground state) which plays an important role in neutral-current neutrino scattering on nuclei relevant to modifications of the electron neutrino spectrum in core collapse supernovae [20]. In hadronic charge-exchange reactions alone it is difficult to extract the GT_0 strength distributions because a superposition of the possible isospin components is measured and a decomposition depends on the availability of a rather complete set of experimental data on $M1$, spin–flip $M1$ and GT strengths [21].

Another important question is the role of the scissors mode in the low-energy $M1$ response of ^{56}Fe. Its properties are well established in heavy nuclei and it has been shown to be well separated from the $M1$ spin–flip resonance and thus of rather pure orbital character [22]. However, in fp-shell nuclei the two modes generally exhibit stronger mixing and an extraction of the scissor mode is thus more complicated [23–25]. Correspondingly, the features of the scissors mode in lighter nuclei are less well explored and ^{56}Fe, with a considerable ground state deformation, represents an interesting candidate.

The present work reports on a study of the $M1$ strength in ^{56}Fe with high-resolution inelastic electron scattering. Emphasis is put on the energy region below the spin–flip resonance where the scissors mode is expected. Some information on $M1$ transitions in ^{56}Fe exists from (γ, γ') studies [26–28]. However, investigation of their momentum transfer dependence provides a deeper insight, in particular into the role of spin–orbit interference effects. Some results of the (e, e′) reaction on mixed-symmetry 2^+ excitations in ^{56}Fe have been published previously [29].

2. Experiments

2.1. Experimental techniques

Two sets of measurements for the reaction ^{56}Fe(e, e′) were carried out, one for low-q values ($q \approx 0.5$ fm^{-1}) and another for the higher-momentum transfer region $q \simeq 0.8$–1.7 fm^{-1}. The low-q measurements were performed at the Darmstadt electron linear accelerator (DALINAC) which is described in detail elsewhere [30], while high-q measurements were performed at the electron accelerator at NIKHEF, Amsterdam [31]. In Darmstadt, inelastically scattered electrons were detected using a 169° double focusing magnetic spectrometer, while in Amsterdam a QDD magnetic spectrometer was used. The kinematical conditions of the measurements are summarized in Table 1. In addition to the spectra of the inelastically scattered electrons, those of the elastically scattered electrons were taken for a normalization of the cross sections and a line shape analysis.

The target used in the present experiment was a self-supporting foil of ^{56}Fe, of 11.66 mg/cm^2 thickness and a purity of 99.93%. Fig. 1 shows the background subtracted electron scattering spectra measured at Darmstadt, while Fig. 2 presents the spectra measured at Amsterdam. Prominent in the spectra is the $M1$ excitation of a state at an excitation energy of 3.449 MeV and several known $E2$ transitions around this energy.

2.2. Data analysis

The spectra were decomposed into peak and background components using the program FIT [32,33] as described by Hofmann et al. [34]. Because of the experimental conditions the shape of the inelastic peaks of one spectrum must be that of the corresponding elastic peak. The line shape parameters were thus determined from the elastic line shape and then kept fixed for the inelastic peak except for the peak area and the peak position. Spectral lines and background were fitted simultaneously. The full peak area was calculated after correction for radiative losses. Energy resolution ranged from 30 to 44 keV, and the absolute uncertainty in excitation energies obtained in this work is estimated to be ± 10 keV.

The inelastic cross sections were extracted from the spectra in the following manner: the area under each fitted peak was divided by the area under the corresponding elastic peak.

Table 1
Kinematical conditions of the ^{56}Fe(e, e′) measurements. The effective momentum transfer q_{eff} is defined in Eq. (2)

E_0 (MeV)	Θ_e (deg)	q_{eff} (fm^{-1})	ΔE (keV)	E_x (MeV)
29.8	141	0.417	32	2.0–9.0
29.9	165	0.436	33	2.0–9.0
41.4	117	0.476	38	2.0–8.5
41.3	165	0.552	35	2.0–9.0
68.6	154	0.811	31	2.0–9.0
107.1	154	1.193	30	2.0–9.0
157.2	154	1.687	44	2.0–9.0

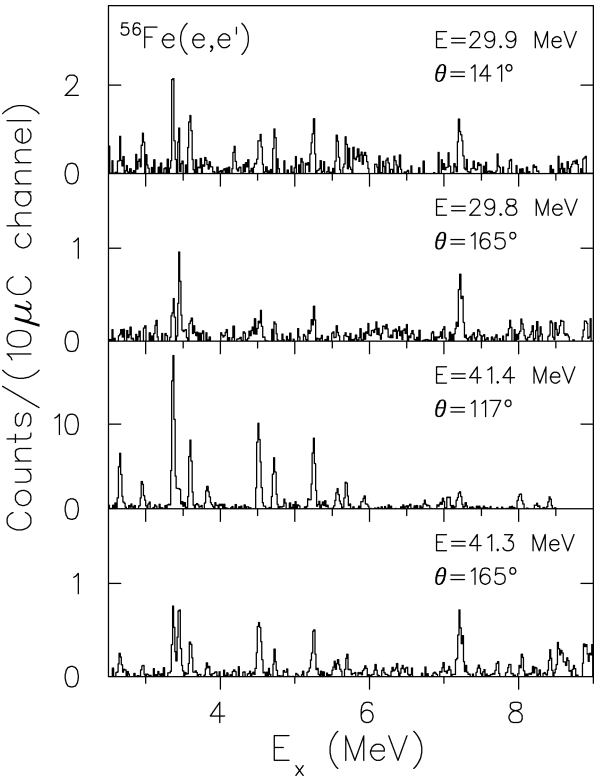

Fig. 1. Background subtracted spectra of the ^{56}Fe(e, e′) reaction measured at the DALINAC.

The ratios were corrected for radiation and spectrometer dispersion effects, and were then multiplied by the theoretical elastic scattering cross sections calculated with the distorted wave Born approximation (DWBA) phase shift method.

From the seven spectra, a consistent set of 18 peaks which could be identified in most spectra was selected for further analysis. A model-independent analysis (see, e.g., [35]) was used in order to establish the multipolarity of the observed transitions and an initial determination of the transition strength. In the plane wave Born approximation (PWBA), the reduced transition strength for longitudinal electric transitions (C) or transverse magnetic transitions (M), of multipolarity L, may be written as a power series in the momentum transfer q

$$\sqrt{\frac{B(XL,q)\uparrow}{B(XL,0)\uparrow}} = 1 + \sum_{\nu=1}^{\infty} b_\nu(XL) R_{\rm tr}^{(2\nu)}(XL) q^{2\nu}, \tag{1}$$

where $X = C, M$ and $L \geqslant 1$. The coefficients $b_\nu(XL)$ are given, e.g., in Ref. [35]. The quantities $R_{\rm tr}$ are weighted moments of the transition charge density and the transition current density (see, e.g., [36]). The quantity $R_{{\rm tr}(XL)} = \sqrt{R_{{\rm tr}^{(2)}}}(XL)$ is called the transition radius. In practice, the ratios $u(XL) = (R_{\rm tr}^{(4)}(XL))^{1/2}/R_{\rm tr}(XL)^2$ and $v(XL) =$

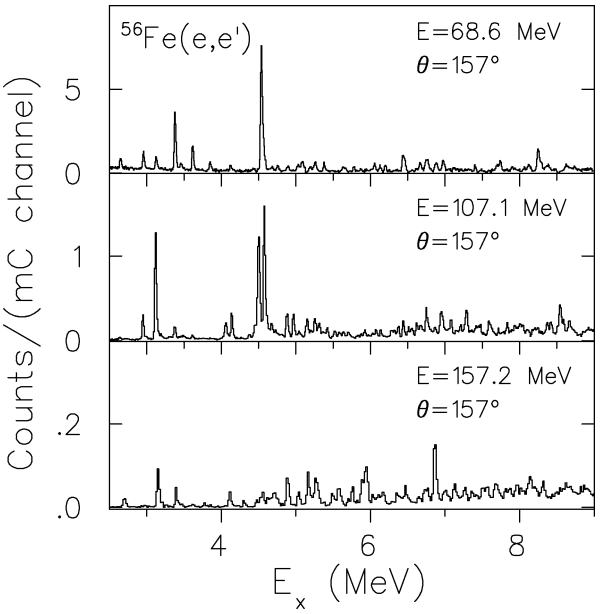

Fig. 2. Background subtracted spectra of the ^{56}Fe(e, e′) reaction measured at the NIKHEF.

$(R_{\rm tr}^{(6)}(XL))^{1/3}/R_{\rm tr}(XL)^2$ vary only slightly for all possible transitions. An average of values was obtained for ^{56}Fe using the program PAMELA [37] and the values were fixed at $u = 1.15$ and $v = 1.26$. The method was applied to the low-q form factor data only, and the series was truncated at $\nu = 3$. The formulation applies in PWBA. In practice the distortion of the wave functions is not negligible and the measured cross sections were corrected by the ratio of PWBA to DWBA cross section extracted from output of the program PAMELA. These correction factors range from 0.72 to 1.66.

Values of $\sqrt{B(XL,q)\uparrow}$ were extracted from the experimental form factors, corrected for distortion, and were fitted to Eq. (1) as a function of q^2 using $\sqrt{B(XL,0)\uparrow}$ and $R_{\rm tr}(XL)^2$ as fitting parameters. Fig. 3 illustrates the procedure for the cases of the states at $E_{\rm x} = 3.449$ MeV and $E_{\rm x} = 4.732$ MeV, with known transitions of $M1$ and $E2$ type, respectively. The fits allow the different multipolarities to be clearly distinguished. This procedure was applied to the transition strengths for all 18 observed levels. The multipolarities assigned are given in Table 2 for the transitions observed in the experiment.

3. DWBA analysis of form factors and $B(M1)$ strengths

For the identified 1^+ levels, the experimental transverse form factors were compared with form factors calculated with DWBA wave functions in order to obtain experimental values for the transition strengths $B(M1)\uparrow$. Input data for the DWBA calculation, in the form of one body transition densities, was obtained from a shell-model calculation. It may

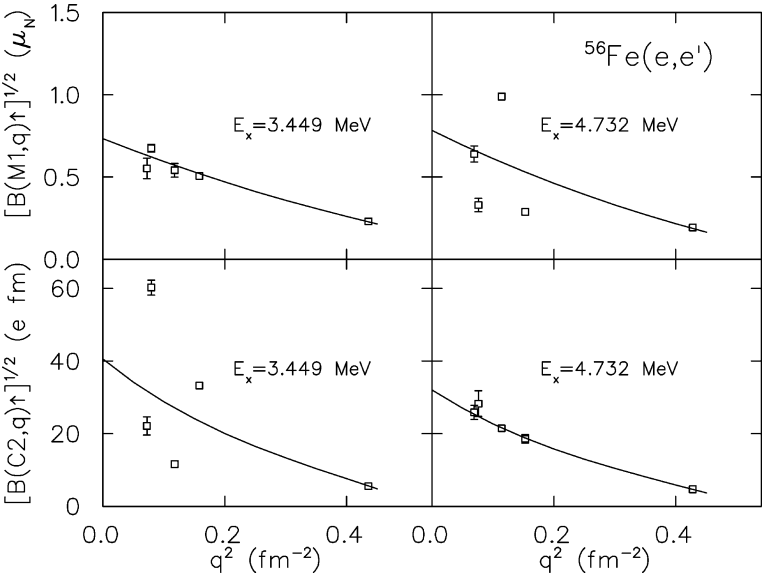

Fig. 3. PWBA analysis of the ^{56}Fe(e, e′) form factors for two examples of transitions to known 1^+ ($E_x = 3.449$ MeV) and 2^+ ($E_x = 4.732$ MeV) states, respectively.

Table 2
Levels observed in the ^{56}Fe(e, e′) experiment. Excitation energies, E_x, and total angular momentum and parities, J^π, are extracted from a model-independent PWBA analysis while the transition strengths $B(M1)\uparrow$ are determined in a model-dependent DWBA analysis using shell-model transition densities

E_x (MeV)	J^π	$B(M1)\uparrow$ (μ_N^2) This work	$B(M1)\uparrow$ (μ_N^2) [28]
2.661	2^+		
2.963	2^+		
3.369	2^+		
3.449	1^+	0.510(51)	0.494(32)
3.599	2^+		
3.816	2^+		
4.539	2^+		
4.732	2^+		
5.255	2^+		
5.571	1^-		
5.692	2^+		
7.071	2^+		
7.209	1^+	0.546(39)	0.425(26)
7.249	1^+	0.224(41)	0.149(23)
7.899	1^+	0.121(23)	0.199(20)
8.056	?		
8.443	$1^+, 2^+$	0.142(37)	
8.895	1^+	0.212(41)	0.238(116)

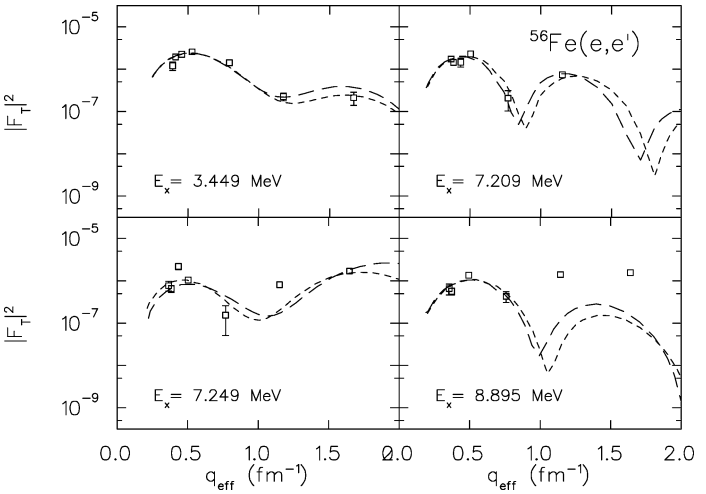

Fig. 4. Examples of the DWBA analysis of $M1$ transitions identified in the ^{56}Fe(e, e′) reaction using shell-model form factors. Results obtained with the FPD6 [39] and FPC8 [40] interactions are shown as short-dashed and long-dashed lines, respectively.

be noted that the DWBA corrections to the cross sections are significant and may reach factors up to two compared to the PWBA analysis discussed in the previous section.

The shell-model calculations were performed using the program OXBASH [38]. The 16 particles outside the $(N, Z = 20, 20)$ shells were described in a restricted fp model space, with possible configurations $(f_{7/2})^{14}(p_{1/2}p_{3/2}f_{5/2})^2$ and $(f_{7/2})^{13}(p_{1/2}p_{3/2}f_{5/2})^3$, i.e., including 2p–2h and 3p–3h excitations (truncation level $t = 3$). Calculations were performed using the FPD6 [39] and FPC8 [40] interactions. An adjusted single particle spectrum is needed for the description of nuclei in the vicinity of the doubly magic ^{56}Ni when using the FPD6 interaction [41]. One-body transition densities were obtained for excitations to $J^\pi = 1^+$ states.

Using these one-body transition densities, DWBA transverse form factors for the model transitions were calculated with the program PAMELA [37]. An effective spin g-factor $g_s^{\text{eff}} = 0.7 g_s^{\text{free}}$ for the proton and neutron was introduced. These form factors were scaled to the experimental data, and the scaled value of the $B(M1)$ transition strength was obtained. Fits for various transitions are illustrated in Fig. 4. The results are shown as a function of the effective momentum transfer q_{eff}

$$q_{\text{eff}} = q\left(1 + \frac{3}{2}\frac{Ze^2}{\hbar c E_0 R_{\text{eq}}}\right), \tag{2}$$

where $R_{\text{eq}} = 1.12 \times A^{1/3}$. The differences of the momentum transfer dependence are clear indicators of differences in the underlying structure of the shown examples. The 1^+ states at 7.209 MeV and 8.895 MeV are typically excited by spin–flip transitions of dominant $1f_{7/2} \to 1f_{5/2}$ type. The state at 3.449 MeV is mainly excited by orbital currents, as discussed in detail below, while the transition to the level at 7.249 MeV is more complex with several relevant contributions.

The set of available shell-model form factors was fitted to each data set and the result with the lowest χ^2 was chosen. Transition strengths extracted using this fitting procedure did not differ significantly for the FPC8 or FPD6 interactions. Thus their results were averaged and taken as the experimental values. Table 2 summarizes the $B(M1)$ strengths of the transitions identified to have $M1$ character in the model independent analysis. The values are compared with the results of Bauwens et al. [28] measured by nuclear resonance fluorescence. The agreement is quite good except for the transitions to the states at 7.249 and 7.899 MeV where the results are just outside the respective error bars. For the transition to the level at 3.449 MeV a further experimental result $B(M1) = 0.62\ \mu_N^2$ has been obtained using the self-absorption technique [42]. A state at 3.120 MeV with likely $J^\pi = 1^+$ assignment has been reported [43] but the g.s. decay width is very weak ($B(M1)\uparrow\ \approx\ 3\times 10^{-3}\ \mu_N^2$) and thus beyond the sensitivity limit of the present experiment.

4. Shell-model description of the $M1$ response in ^{56}Fe

As demonstrated in Fig. 5, the $M1$ strength distribution in ^{56}Fe below the spin–flip resonance provides a sensitive test case for different shell-model interactions. The top part of Fig. 5 displays the experimental $B(M1)$ strengths deduced with the methods described in the previous section. In the second and third row results obtained with the FPC8 and FPD6 interactions, respectively, in the $t = 3$ model space discussed above are presented. The most prominent transition at 3.449 MeV is reasonably well described in energy and absolute $B(M1)$ value by both. The experimental sensitivity limit is of the order $B(M1) \approx 0.1\ \mu_N^2$. Thus, $M1$ transitions as predicted in the excitation-energy range $E_x \simeq 4$–7 MeV by the FPC8 results are largely excluded, while weaker transitions as predicted by FPD6 may be possible. The two strong transition just above 7 MeV are found at the right energy in the FPD6 results while the corresponding group is shifted to about 6.5 MeV in the FPC8 calculation. The $M1$ strength is underestimated in both cases but even more severe in the distribution generated with FPD6.

It may also be noted that a calculation in a (2p–2h) configuration space using an interaction derived from the G matrix has been reported earlier [44]. A study of the possible mixed-symmetry character (within the interacting boson model-2) of low-lying 1^+ states predicts a splitting in two levels at $E_x \approx 3.5$ MeV [45] which is not observed in the present experiment, in line with the experimental findings of [28]. However, the total g.s. $B(M1)$ strength predicted for both excitations agrees well with experiment.

It is interesting to compare the experimental observations to a larger space fp-shell calculation presented in the bottom part of Fig. 5. We performed calculations using the code NATHAN [46]. NATHAN has been developed in the jj-coupling scheme using the quasispin formalism. We adopted a version of the code adapted to shared-memory parallel machines. The calculation has been performed within the full fp shell allowing a maximum of 4 particles to be promoted from the $f_{7/2}$ orbital to the rest of the shell ($p_{3/2,1/2}$, $f_{5/2}$), i.e., truncation level $t = 4$. At this truncation level $B(M1)$ strength distributions are virtually converged. We checked this by performing a truncation level $t = 3$ calculation and observed a reduction of 5% in the total $B(M1)$ strength by going from $t = 3$ to $t = 4$. The KB3G interaction was used, an improved version of the standard

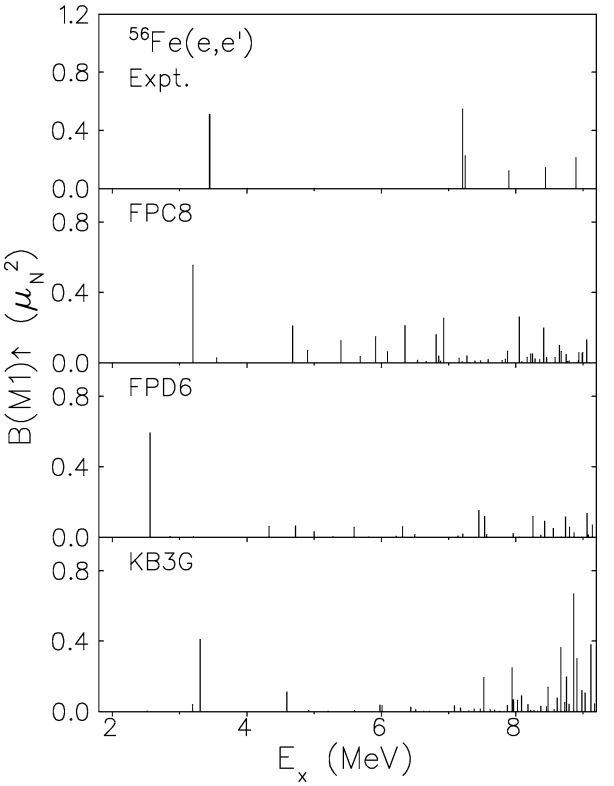

Fig. 5. Experimental $B(M1)$ strength distribution in ^{56}Fe below 9 MeV in comparison with shell-model calculations in a 3p–3h space using the FPC8 [40] and FPD6 [39] effective interactions, respectively, and a 4p–4h calculation using the KB3G interaction.

KB3 interaction which corrects the latter for some slight shortcomings around the $N = 28$ shell gap [47]. We have calculated the individual orbital and spin contributions to the $M1$ strength distributions as well as the total $B(M1)$ strength. As above, an effective spin g-factor $g_s^{\text{eff}} = 0.7 g_s^{\text{free}}$ has been adopted. To allow for a detailed comparison with the high-resolution data, all strength distributions have been obtained after 400 Lanczos iterations.

The prominent low-energy transition is well described although the $B(M1)$ value of 0.41 μ_N^2 is slightly below the experimental value of 0.51 μ_N^2. There is a general tendency to smaller $B(M1)$ values than found in the experiment. A counterpart to the theoretically predicted excitation of the 1^+ state at 4.596 MeV may be masked in the experiment by close-lying prominent $E2$ transitions. For excitation energies above 8 MeV large differences are visible between the three shell-model results. It has been discussed in the neighboring ^{54}Fe and other $N = 28$ isotones that sufficiently large model spaces are needed for a realistic description of the $M1$ spin–flip resonance [3]. Obviously a 3p–3h model space is not yet sufficient to give a realistic picture of the fine structure of the $M1$ strength (or the corresponding GT strength) in this energy region while a calculation using the full $0\hbar\omega$ space is expected to do so for a sufficient number of Lanczos iterations.

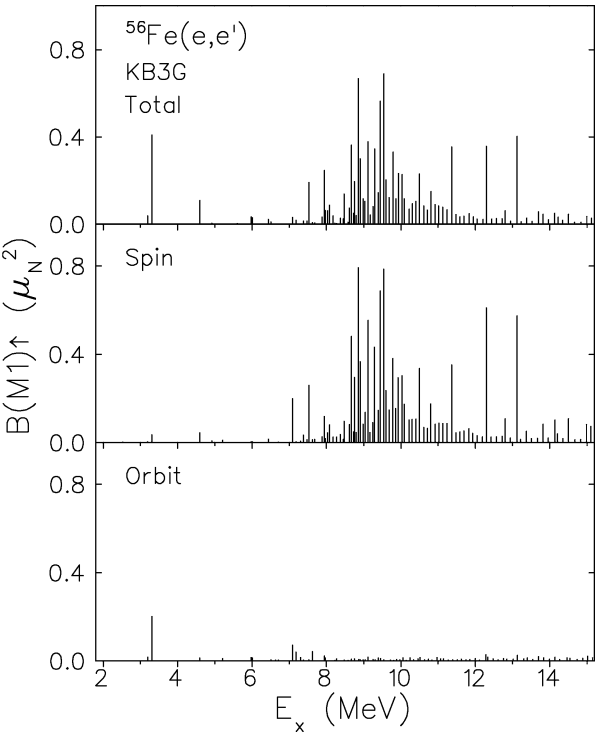

Fig. 6. Shell-model $M1$ strength distribution obtained in a 4p–4h space with the KB3G interaction [47] extended up to 15 MeV including the spin–flip resonance and its separation into spin and orbital contributions.

The role of spin and orbital currents are qualitatively similar in all three calculations for excitation energies up to 7 MeV. As an example, a decomposition of the 4p–4h space results with the KB3G interaction is shown in Fig. 6 which should also give a realistic picture in the spin–flip regime. Orbital contributions are important below 8 MeV and mostly constructive interference with spin matrix elements is found. At higher excitation energies, spin excitations dominate and the much smaller orbital contributions mainly interfere destructively. In the region between 7 and 8 MeV, a concentration of orbital but very little total $M1$ strength is predicted due to a large cancellation with spin contributions. An interesting feature of the theoretical $M1$ distribution are four very strong spin transitions at high excitation energies (i.e., high level densities) between 10 and 14 MeV. These can be understood to arise from isospin conservation because the corresponding 1^+ states have isospin $T = T_0 + 1$. It is interesting to note that this behavior is confirmed in great detail in an ^{56}Fe(p, p) experiment at very forward angles ($\Theta = 2.8°$) and for an incident proton energy $E_p = 280$ MeV [48]. For these kinematical conditions $\Delta L = 0$ spin–isospin–flip excitations populating 1^+ states are favored in proton scattering.

The absolute value of the dominantly orbital transition at 3.449 MeV, which carries a large fraction of the scissors mode, is very sensitive to the predictions of spin/orbit matrix element ratios $M_{L,S}$ (given by $B(M1) = [M_L \pm M_S]^2$) in the various models.

Table 3
Spin and orbital matrix elements $M_{L,S}$ and their ratio R predicted by the shell-model calculations described in the text for the prominent scissors mode transition in ^{56}Fe

Interaction	M_L (μ_N)	M_S (μ_N)	R	$B(M1)\uparrow$ (μ_N^2)
FPC8	0.51	0.24	2.18	0.56
FPD6	0.52	0.27	1.94	0.62
KB3G	0.45	0.19	2.58	0.41
Experiment				0.51

A decomposition for the calculations discussed above is presented in Table 3. The FPD6 and FPC8 results show almost identical orbital matrix elements but differ in the spin contribution, and accordingly in the predicted orbital-to-spin ratio R, where values around 2 are found. The predictions of the KB3G calculation are consistently smaller for M_L and M_S and a larger R value of about 2.6 is predicted. This may be compared to experimental findings of $R \approx 1$ in ^{46}Ti and $R > 4$ in deformed rare-earth nuclei [49].

Investigations of the scissors mode in heavy nuclei have demonstrated the sensitivity of electron scattering form factors to the difference between $M1$ transitions governed by orbital or spin excitations [50–52]. It is instructive to look at the same question in lighter nuclei like ^{56}Fe where the mixing is generally more pronounced. By way of example we use in Fig. 7 the FPC8 (upper part) and KB3G (lower part) shell-model results to investigate this question for the transition to the state at 3.449 MeV. The long-dashed (short-dashed) lines show the result obtained by setting the spin (orbital) g-factor to zero in the form factor calculation. The solid lines represent the full results including the cross terms. Clearly, the orbital/spin ratio shows a pronounced momentum transfer dependence which allows a test of the microscopic calculations beyond the $B(M1)$ strength distributions deduced at the photon point.

The orbital part of the FPC8 result exhibits a smooth q dependence while the spin part shows pronounced minima at $q_{\text{eff}} \approx 0.8$ and 1.2 fm^{-1}. From the ratio of the total and orbital form factor one can easily see that the interference sign changes from positive at low q to negative in the vicinity of the second maximum of the spin form factor again to positive near the third maximum. The spin form factor differs considerably from those of prominent spin–flip excitations around $E_x \simeq 8$ MeV shown in Fig. 4. While the latter are dominated by the $1f_{7/2} \rightarrow 1f_{5/2}$ transition, the spin strength mixed into the scissors mode state form factor is mainly generated by transitions between the $2p$ states.

The form factors obtained with the KB3G calculation are comparable for $q_{\text{eff}} \leqslant 0.8$ fm^{-1}. The spin–flip part looks qualitatively similar to the FPC8 result although the second maximum is shifted to a slightly higher value $q_{\text{eff}} \simeq 1.5$ fm^{-1}. However, significant differences are observed for the q dependence of the orbital strength. For $q > 1$ fm^{-1} it is much weaker and exhibits a minimum similar to the spin–flip contribution. Furthermore, the interference is generally destructive for these higher momentum transfers including the region of the second maximum. As a result the experimental form factor at high q is underpredicted by factors up to an order of magnitude while the FPC8 calculation accounts quite well for the data.

Finally, the well established relation between deformation and scissors mode strength is discussed briefly for the present case. Application of the phenomenological sum

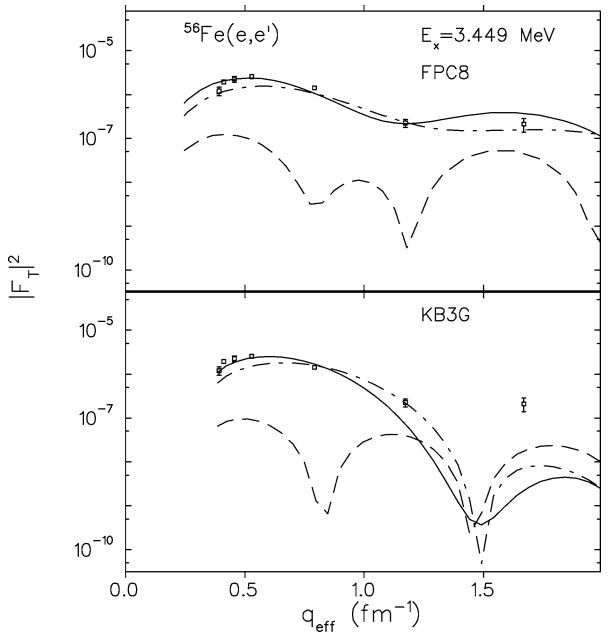

Fig. 7. Form factors of the scissors mode transition at $E_x = 3.449$ MeV. The data (open squares) are compared with the predictions of shell-model calculations described in the text using the FPC8 (upper part) and KB3G (lower part) interactions. The dashed and dashed-dotted lines are the separated spin and orbital parts, respectively, and the solid lines show the full results including the cross-terms.

rule presented in [9] leads to the following predictions for ^{56}Fe: total low-energy scissors mode strength $\sum B(M1) = 0.35\ \mu_N^2$ and energy centroid $E_{sc} = 4.49$ MeV. However, any comparison to experimental results is complicated by the strong interference with spin admixtures. Analyzing the different shell-model results, a varying degree of correspondence is found which is particularly sensitive to the group of $M1$ transitions with large orbital matrix elements predicted around 6–7 MeV. A more quantitative analysis would require measurements of the corresponding spin $M1$ matrix elements, e.g., with 0° inelastic proton scattering.

5. Summary and concluding remarks

The present work has focused on an experimental investigation of the $M1$ strength in ^{56}Fe below the main spin–flip resonance with high-resolution inelastic electron scattering. Data taken at the DALINAC at low q have been complemented by measurements at NIKHEF for momentum transfers up to about 1.7 fm^{-1}. A $B(M1)$ strength distribution has been deduced by a DWBA analysis of the form factors using shell-model wave functions. The low-lying $M1$ strength turns out to be a very sensitive test of different shell-model approaches. It is found that a full $0\hbar\omega$ calculation is not necessarily superior to results

obtained in the restricted, but sufficiently large (in the present case 3p–3h) model spaces. The choice of the residual interaction seems to be more important.

All shell-model results agree that the prominent transition at 3.449 MeV carries a major fraction of the scissors mode in ^{56}Fe. However, because spin contributions are generally larger in fp-shell nuclei compared, e.g., to the rare earth region, its $B(M1)$ strength is particularly sensitive to the ratio of orbital and spin matrix elements. The form factor exhibits a strong momentum transfer dependence of the spin/orbit mixing, which at large q differs considerably from that at the photon point and thus serves as an experimental proof of the dominantly orbital nature. A group of $M1$ transitions with rather strong orbital contributions is predicted between 7 and 8 MeV. However, destructive interference leads to absolute $B(M1)$ values that are probably too small to be observed in the present experiments.

Future interest should also focus on the spin–flip resonance region. The spin–flip $M1$ response provides a measure for the GT_0 strength relevant in neutrino–nucleus interactions during a supernova shock wave [20]. Generally, as complete as possible data sets on the $M1$ response from high-resolution electromagnetic and hadronic reactions are of high interest because they permit a full test of spin and orbital $M1$ modes and their interference pattern in state-of-the-art microscopic model calculations. Thus, it would be worthwhile to extend the (e, e′) experiments to higher excitation energies and a better mapping of the momentum transfer dependence and combine it with high-resolution charge exchange and inelastic proton scattering data which can be obtained, e.g., at the detector of EUROSUPERNOVA Collaboration [53,54] at KVI, Groningen or the new high-resolution facility at RCNP, Osaka [55,56], and maybe also in future at iThembaLABS, Somerset West [57].

Acknowledgements

Discussions with F. Bauwens, D. Frekers, E. Jacobs and H.J. Wörtche are acknowledged. R.W.F. expresses his thanks to the Darmstadt group for the kind hospitality experienced during several visits where the present work was initiated.

References

[1] F. Osterfeld, Rev. Mod. Phys. 64 (1992) 491.
[2] G. Martinez-Pinedo, A. Poves, E. Caurier, A.P. Zuker, Phys. Rev. C 53 (1996) R2602.
[3] P. von Neumann-Cosel, A. Poves, J. Retamosa, A. Richter, Phys. Lett. B 443 (1998) 1.
[4] A. Richter, A. Weiss, O. Häusser, B.A. Brown, Phys. Rev. Lett. 65 (1990) 2519.
[5] C. Lüttge, P. von Neumann-Cosel, F. Neumeyer, C. Rangacharyulu, A. Richter, G. Schrieder, E. Spamer, D.I. Sober, S.K. Matthews, B.A. Brown, Phys. Rev. C 53 (1996) 127.
[6] P. von Neumann-Cosel, A. Richter, Y. Fujita, B.D. Anderson, Phys. Rev. C 55 (1997) 532.
[7] D. Bohle, A. Richter, W. Steffen, A.E.L. Dieperink, N. Lo Iudice, F. Palumbo, O. Scholten, Phys. Lett. B 137 (1984) 27.
[8] W. Ziegler, C. Rangacharyulu, A. Richter, C. Spieler, Phys. Rev. Lett. 65 (1990) 2515.
[9] J. Enders, H. Kaiser, P. von Neumann-Cosel, C. Rangacharyulu, A. Richter, Phys. Rev. C 59 (1999) R1851.
[10] D. Zawischa, J. Phys. G 24 (1998) 683.
[11] N. Lo Iudice, Riv. Nuovo Cimento 23 (2000) 1.

[12] K. Langanke, M. Wiescher, Rep. Prog. Phys. 64 (2001) 1657.
[13] D.J. Dean, P.B. Radha, K. Langanke, Y. Alhassid, S.E. Koonin, W.E. Ormand, Phys. Rev. Lett. 72 (1994) 4066.
[14] E. Caurier, G. Martinez-Pinedo, A. Poves, A.P. Zuker, Phys. Rev. C 52 (1995) R1736.
[15] P.B. Radha, D.J. Dean, S.E. Koonin, K. Langanke, P. Vogel, Phys. Rev. C 56 (1997) 3079.
[16] E. Caurier, K. Langanke, G. Martinez-Pinedo, F. Nowacki, Nucl. Phys. A 653 (1999) 439.
[17] K. Langanke, G. Martinez-Pinedo, Nucl. Phys. A 673 (2000) 481.
[18] J. Rapaport, T. Taddeucci, T.P. Welch, C. Gaarde, J. Larsen, D.J. Horen, E. Sugarbaker, P. Koncz, C.C. Foster, C.D. Goodman, C.A. Goulding, T. Masterson, Nucl. Phys. A 410 (1983) 371.
[19] S. El-Kateb, K.P. Jackson, W.P. Alford, R. Abegg, R.E. Azuma, B.A. Brown, A. Celler, D. Frekers, O. Häusser, R. Helmer, R.S. Henderson, K.H. Hicks, R. Jeppesen, J.D. King, K. Raywood, G.G. Shute, B.M. Spicer, A. Trudel, M. Vetterli, S. Yen, Phys. Rev. C 49 (1994) 3128.
[20] J.M. Sampaio, K. Langanke, G. Martinez-Pinedo, D.J. Dean, Phys. Lett. B 529 (2002) 19.
[21] Y. Fujita, H. Akimune, I. Daito, M. Fujiwara, M.N. Harakeh, T. Inomata, J. Jänecke, K. Katori, H. Nakada, S. Nakayama, A. Tamii, M. Tanaka, H. Toyokawa, M. Yosoi, Phys. Lett. B 365 (1996) 29.
[22] A. Richter, Prog. Part. Nucl. Phys. 34 (1995) 261.
[23] L. Zamick, Phys. Rev. C 31 (1985) 1955.
[24] M. Abdelaziz, J.P. Elliott, Phys. Lett. B 187 (1987) 505.
[25] A. Richter, Nucl. Phys. A 507 (1990) 99c.
[26] T. Chapuran, R. Starr, R. Vodhanel, M.K. Brussel, Phys. Rev. C 30 (1984) 54.
[27] B.S. Ishkhanov, I.M. Kapitonov, A.Yu. Ugaste, V.I. Shvedunov, E.V. Shirokov, Phys. At. Nucl. 57 (1994) 2041.
[28] F. Bauwens, J. Bryssinck, D. De Frenne, K. Govaert, L. Govor, M. Hagemann, J. Heyse, E. Jacobs, W. Mondelaers, V.Yu. Ponomarev, Phys. Rev. C 62 (2000) 024302.
[29] G. Hartung, A. Richter, E. Spamer, H.J. Wörtche, C. Rangacharyulu, C.W. de Jager, H. de Vries, Phys. Lett. B 221 (1989) 109.
[30] H.-D. Gräf, H. Miska, E. Spamer, O. Titze, T. Walcher, Nucl. Instrum. Methods 153 (1978) 9;
T. Walcher, R. Frey, H.-D. Gräf, E. Spamer, H. Theissen, Nucl. Instrum. Methods 153 (1978) 17;
D. Schüll, J. Foh, H.-D. Gräf, H. Miska, R. Schneider, E. Spamer, H. Theissen, O. Titze, T. Walcher, Nucl. Instrum. Methods 153 (1978) 29;
J. Foh, R. Frey, R. Schneider, D. Schüll, A. Schwierczinski, H. Theissen, O. Titze, Nucl. Instrum. Methods 153 (1978) 48.
[31] C. de Vries, C.W. de Jager, L. Lapikas, G. Luijckx, R. Maas, H. de Vries, P.K.A. de Witt Huberts, Nucl. Instrum. Methods A 223 (1984) 1.
[32] S. Strauch, Diploma Thesis, Technische Hochschule Darmstadt, 1993.
[33] F. Neumeyer, Diploma Thesis, Technische Hochschule Darmstadt, 1993.
[34] F. Hofmann, P. von Neumann-Cosel, F. Neumeyer, C. Rangacharyulu, B. Reitz, A. Richter, G. Schrieder, D.I. Sober, L.W. Fagg, B.A. Brown, Phys. Rev. C 65 (2002) 024311.
[35] T. Guhr, H. Diesener, A. Richter, C.W. de Jager, H. de Vries, P.K.A. de Witt Huberts, Z. Phys. A 336 (1990) 159.
[36] P. von Neumann-Cosel, H.-D. Gräf, U. Krämer, A. Richter, E. Spamer, Nucl. Phys. A 669 (2000) 3.
[37] N.I. Kassis, W. Knüpfer, private communication.
[38] B.A. Brown, A. Etchegoyan, W.D.M. Rae, N.S. Godwin, W.A. Richter, C.H. Zimmerman, W.E. Ormand, J.S. Winfield, MSU-NSCL Report No. 524, 1985.
[39] W.A. Richter, M.G. van der Merwe, R.E. Julies, B.A. Brown, Nucl. Phys. A 523 (1991) 325;
W.A. Richter, M.G. van der Merwe, R.E. Julies, B.A. Brown, Nucl. Phys. A 577 (1994) 585.
[40] W.A. Richter, M.G. van der Merwe, B.A. Brown, Nucl. Phys. A 586 (1995) 445.
[41] P. von Neumann-Cosel, A. Richter, C. Schlegel, R. Schulz, Nucl. Phys. A 650 (1999) 267.
[42] B.S. Ishkhanov, I.M. Kapitonov, E.V. Shirokov, B.A. Yurev, L.I. Govor, A.M. Demidov, Phys. At. Nucl. 61 (1998) 515.
[43] J. Huo, Nucl. Data Sheets 86 (1999) 315.
[44] H. Nakada, T. Sebe, T. Otsuka, Nucl. Phys. A 571 (1994) 467.
[45] H. Nakada, T. Otsuka, Phys. Rev. C 55 (1997) 2418.

[46] E. Caurier, G. Martinez-Pinedo, F. Nowacki, A. Poves, J. Retamosa, A.P. Zuker, Phys. Rev. C 59 (1999) 2033.
[47] A. Poves, J. Sanchez-Solano, E. Caurier, F. Nowacki, Nucl. Phys. A 694 (2001) 157.
[48] D. Frekers, H.J. Wörtche, private communication.
[49] C. Djalali, N. Marty, M. Morlet, A. Willis, J.C. Jourdain, D. Bohle, U. Hartmann, G. Küchler, A. Richter, G. Caskey, G.M. Crawley, A. Galonsky, Phys. Lett. B 164 (1985) 269.
[50] F.G. Scholtz, R. Nojarov, A. Faessler, Phys. Rev. Lett. 63 (1989) 1356.
[51] N. Lo Iudice, F. Palumbo, A. Richter, H.J. Wörtche, Phys. Rev. C 42 (1990) 241.
[52] A. Richter, Nucl. Phys. A 522 (1991) 139c.
[53] S. Rakers, F. Ellinghaus, R. Bassini, C. Bäumer, A.M. van den Berg, D. Frekers, D. De Frenne, M. Hagemann, V.M. Hannen, M.N. Harakeh, M. Hartig, R. Henderson, J. Heyse, M.A. de Huu, E. Jacobs, M. Mielke, J.M. Schippers, R. Schmidt, S.Y. van der Werf, H.J. Wörtche, Nucl. Instrum. Methods A 481 (2002) 253.
[54] S. Rakers, C. Bäumer, D. Frekers, R. Schmidt, A.M. van den Berg, V.M. Hannen, M.N. Harakeh, M.A. de Huu, H.J. Wörtche, D. De Frenne, M. Hagemann, J. Heyse, E. Jacobs, Y. Fujita, Phys. Rev. C 65 (2002) 044323.
[55] H. Fujita, Y. Fujita, G.P.A. Berg, A.D. Bacher, C.C. Foster, K. Hara, K. Hatanaka, T. Kawabata, T. Noro, H. Sakaguchi, Nucl. Instrum. Methods A 484 (2002) 17.
[56] Y. Fujita, H. Fujita, T. Adachi, G.P.A. Berg, E. Caurier, H. Fujimura, K. Hara, K. Hatanaka, Z. Janas, J. Kamiya, T. Kawabata, K. Langanke, G. Martinez-Pinedo, T. Noro, E. Roeckl, Y. Shimbara, T. Shinada, S.Y. van der Werf, M. Yoshifuku, M. Yosoi, R.G.T. Zegers, Eur. Phys. J. A 13 (2002) 411.
[57] J. Carter, R.W. Fearick, S.V. Förtsch, H. Fujita, J.J. Lawrie, P. von Neumann-Cosel, R. Neverling, A. Richter, A. Shevchenko, F.D. Smit, N. Thantcha, Proposal for a high-resolution 0° facility at the K600 spectrometer at the iThembaLABS cyclotron, 2003.